Experimental demonstration of a broadband all-dielectric metamaterial perfect reflector

Parikshit Moitra, Brian A. Slovick, Zhi Gang Yu, S. Krishnamurthy, and Jason Valentine

Citation: Appl. Phys. Lett. **104**, 171102 (2014); doi: 10.1063/1.4873521
View online: https://doi.org/10.1063/1.4873521
View Table of Contents: http://aip.scitation.org/toc/apl/104/17
Published by the American Institute of Physics

Experimental demonstration of a broadband all-dielectric metamaterial perfect reflector

Parikshit Moitra,[1] Brian A. Slovick,[2] Zhi Gang Yu,[2] S. Krishnamurthy,[2] and Jason Valentine[3,a)]
[1]*Interdisciplinary Materials Science Program, Vanderbilt University, Nashville, Tennessee 37212, USA*
[2]*Applied Optics Laboratory, SRI International, Menlo Park, California 94025, USA*
[3]*Department of Mechanical Engineering, Vanderbilt University, Nashville, Tennessee 37212, USA*

(Received 19 February 2014; accepted 10 April 2014; published online 29 April 2014)

All-dielectric metamaterials utilizing Mie resonances in high-permittivity dielectric resonators offer a low-loss alternative to plasmonic metamaterials. Here we present the demonstration of a single-negative all-dielectric metamaterial, comprised of a single layer of cylindrical silicon resonators on a silicon-on-insulator substrate, that possesses peak reflectance over 99% and an average reflectance over 98% across a 200 nm wide bandwidth in the short-wavelength infrared region. The study is also extended to disordered metamaterials, demonstrating a correlation between the degree of disorder and the reduction in reflectance. It is shown that near-unity reflection is preserved as long as resonator interaction is avoided. Realization of near-unity reflection from disordered metamaterials opens the door to large-area implementations using low-cost self-assembly based fabrication techniques. © *2014 AIP Publishing LLC*.
[http://dx.doi.org/10.1063/1.4873521]

Metamaterials (MMs) are artificially fabricated structures that exhibit unique optical properties not existing in Nature, such as negative,[1–5] ultra high,[6] and zero-refractive index.[7,8] Traditionally, MMs have been formed using metal-based unit cells[9] in which conduction current is used to realize high-frequency magnetic and electric resonances for manipulating the effective permeability and permittivity, respectively, of the composite. One of the main limitations in metal-based MMs has been the presence of ohmic damping which results in absorption.[9–11] Moreover, as the plasmon resonance frequency is approached, the kinetic induction of the electrons in the metal results in saturation of the magnetic response, limiting the use of metal-based MMs at high frequencies.[12]

In an effort to overcome these issues, researchers have focused on replacing metallic unit cells[9] with all-dielectric counterparts[13–19] possessing strong Mie resonances.[20] The use of transparent all-dielectric unit cells effectively eliminates ohmic loss and allows one to achieve electric and magnetic resonances using simple unit cell geometries such as spheres, cubes, cylinders, and rods.[7,13,14,21,22] Overlapping of the electric and magnetic resonance have led to the demonstration of double-negative or left handed metamaterials,[13,23] impedance matched zero-index-metamaterials,[7] and complete suppression of resonant backscattering.[21,24] Spectral separation of the resonances can also be used to realize single-negative metamaterials in which either the permittivity, ε, or permeability, μ, is less than zero, while the other component remains positive. In recent work,[25] a single-negative all-dielectric MM was predicted to possess near-unity broadband reflection at optical frequencies. Concurrently, very high reflection (>99%) was observed in the near-infrared region with a suspension of silicon (Si) nanospheres.[26] Perfect reflectors would be useful to protect surfaces against high-power irradiation, as low-loss mirrors in laser cavities, and for generating electric-field nodes to enhance signal-to-noise ratios in bio-imaging and nanosensing.[27] Although Bragg reflectors[28] may be used for such applications, the possibility of achieving disorder-tolerant perfect reflection from a single layer of MM offers several important advantages, including simplified fabrication and the possibility to develop paint-like MM coatings for large-area optics such as those found in reflective telescopes.

In this Letter, we describe the design and fabrication of MM perfect reflectors that utilize Si cylinder resonators. These single-negative MMs exploit the separation between electric and magnetic resonances to realize a broadband reflector in the telecommunications band. Furthermore, by introducing varying degrees of lattice disorder, it is found that near-unity reflection is preserved as long as resonator coupling is avoided, potentially opening the door to their realization using large-scale patterning and fabrication methods such as nanosphere lithography.[29,30]

The conditions to achieve perfect reflection from a homogeneous medium are derived elsewhere[25] and the basic principles are described here for continuity. For a semi-infinite medium, it can be shown that the reflectance is unity when the real part of the impedance of the medium is zero. This condition is achieved when $\varepsilon'/\mu' < 0$ and $\varepsilon''\mu' = \varepsilon'\mu''$, where the complex permittivity and permeability are given by $\varepsilon' + i\varepsilon''$ and $\mu' + i\mu''$, respectively. The first condition requires that the real parts of the permittivity and permeability have opposite signs, which is readily met in the vicinity of an electric or magnetic resonance, provided that the resonances are spectrally isolated. While the second condition is more restrictive, it is readily satisfied in lossless materials. To achieve near-unity reflection with a finite thickness slab, the condition on the impedance is unchanged, but the

a)Email: jason.g.valentine@vanderbilt.edu

imaginary part of the index (n'') must also be maximized to prevent evanescent tunneling across the slab. With this analysis as a guideline, we can begin to design perfect reflecting MMs using the Mie resonances in dielectric particles. In the work presented here, we utilize the cylinder resonator geometry due to its amenability with top-down fabrication techniques. For a cylinder resonator, the positions of the magnetic and electric dipole modes are a function of the aspect ratio (AR), defined as $AR = H/D$, where H is the height of the cylinder and D is the diameter. To demonstrate this dependence, scattering cross-sections for single Si ($\varepsilon = 12$) cylinder resonators embedded in air are plotted in Fig. 1(a) for two different ARs (1.25 and 0.6), where the maxima in electric and magnetic cross sections indicate the positions of the electric and magnetic modes, respectively. The cross-sections were extracted from the far-field scattering profiles of the resonators, wherein the modes are identified as electric and magnetic based on the field profile.[31,32] More information on this technique is given in Section S1 and Fig. S1 of the supplementary material.[33]

To illustrate the spectral separation of electric and magnetic modes across a larger domain, respective mode positions are plotted against the AR in Fig. 1(b). At low ARs, we find that the electric mode is the first resonance and increasing the AR results in a mode crossing. Further increasing the AR results in spectral separation of the modes with the largest spacing occurring at an $AR \sim 1.0$. After this point, increasing the AR results in slight reduction of the spectral separation and eventual saturation in the spacing of the modes. To better understand the collective response of a MM formed from these resonators, the reflectance of an array of resonators is shown in Fig. 1(c). As expected, the reflectance bandwidth is maximized at ARs corresponding to the largest separation between the modes. Furthermore, as the AR is reduced complete modal overlap occurs, leading to a wavelength at which the resonator is impedance matched to air and the appearance of a narrow transmission window. This effect has previously been studied for cylinder resonators as way to achieve complete suppression of backscattering.[24] At $AR \sim 1.0$, there is also a slight dip in the middle of the reflectance band. This dip can be understood by the fact that this region is far from either resonance and thus $|\varepsilon|$ and $|\mu|$ are small, reducing the magnitude of n'' and thus reducing the strength of the reflectance band. Large ARs also result in weakening of the electric and magnetic dipole resonances and a subsequent reduction in the bandwidth of the response. In the design of broadband reflectors, caution must therefore be taken to ensure that spectral separation between the modes and weakening of the resonances does not adversely affect the average reflection across the band.

With these studies as a guideline, we have chosen a Si cylinder resonator-based MM with $H = 500$ nm, $D = 400$ nm ($AR = 1.25$), and a periodicity of 660 nm for experimental studies. This particular AR and cylinder geometry was chosen as it preserves a broad reflection band while also ensuring that the band's position remains within the measurable range of our microscopy setup. It should also be noted that in experimental studies, H was constrained by the wafers used to realize the MMs, as outlined below. To better understand the MM's response, full-wave simulations were performed using the Floquet mode solver in the commercial frequency-domain code HFSS (Ansys) and S-parameter retrieval[34–36] was used to extract the effective optical properties. These simulations were performed for Si resonators, in air, with a permittivity equal to that of our experimental samples which was measured with spectroscopic ellipsometry. As illustrated in Figs. 2(a) and 2(b), the MM is single negative with $\varepsilon' < 0$ and $\mu' > 0$ between 1315 nm and 1500 nm. This leads to an extreme impedance mismatch with $z' = 0$ across this bandwidth, as shown in Fig. 2(c). Within this region, n'' also remains high, satisfying the conditions outlined above and resulting in a band of near-unity reflection as shown in Fig. 2(d), with a peak reflectance of 99.9% at 1450 nm.

The designed MMs were realized by fabricating cylinder resonators in the crystalline Si device layer of a silicon-on-insulator (SOI) wafer (SOItech). The SOI wafers consisted of a Si handle wafer, a 2 μm thick buried silicon oxide layer (SiO_2), and a 500 nm thick crystalline Si device layer. Electron beam lithography (EBL) was used to define the circular mask patterns in polymethyl methacrylate (PMMA) which was spun on top of the Si device layer. This PMMA mask was used to create a 40 nm thick chromium (Cr) mask, defining cylinders, using a lift-off process. The device layer of the wafers was then etched using reactive ion etching

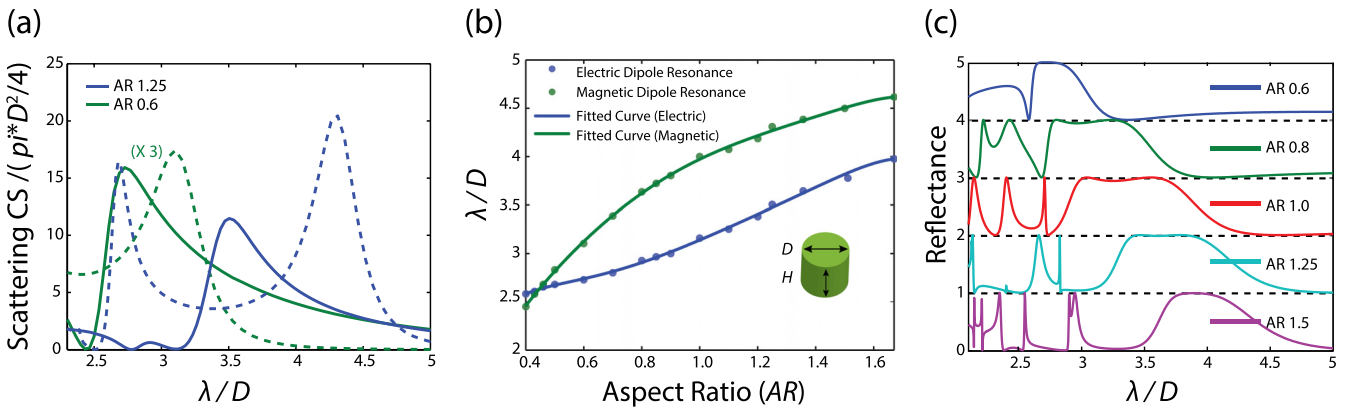

FIG. 1. (a) Scattering cross-sections of single Si ($\varepsilon = 12$) cylinder resonators embedded in an air background for two different aspect ratios ($AR = 1.25$ and $AR = 0.6$). Solid and dashed lines represent the electric and magnetic contributions to the scattering cross-section, respectively. (b) Spectral positions of the electric and magnetic dipole Mie resonances as a function of the AR. The solid lines are fitted to the points as a guide for the eye. (c) Simulated reflectance plots for periodic Si cylinder MMs, illustrating reflectance as a function of cylinder AR.

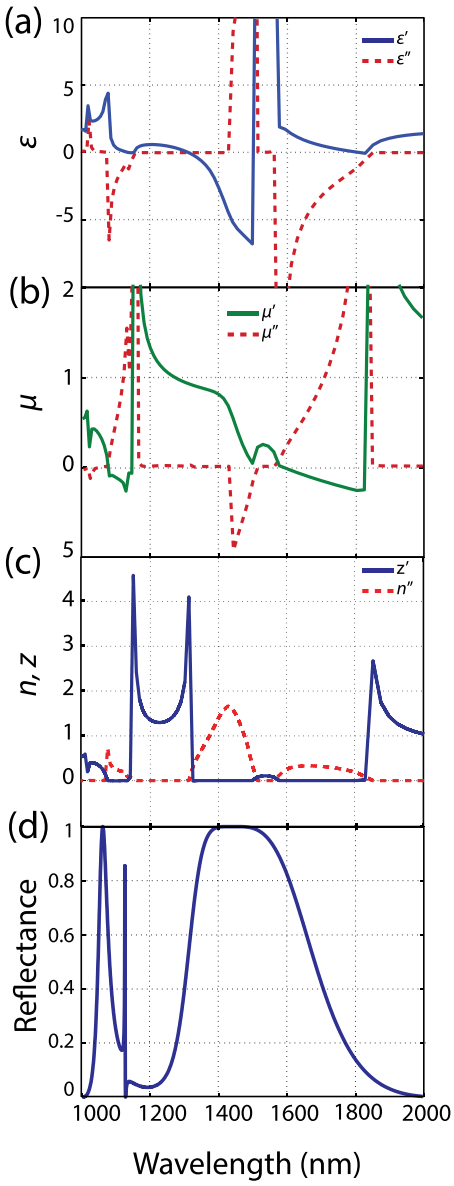

FIG. 2. (a) Effective permittivity and (b) permeability of a periodic cylinder resonator-based MM in an air background with a resonator geometry corresponding to $D = 400$ nm, $H = 500$ nm, and a periodicity of 660 nm. (c) Retrieved n'' and z' for the periodic MM. (d) Reflectance of the MM array numerically calculated using HFSS. A 100 nm near-perfect reflectance band is achieved (reflectance >99%) from 1398 to 1498 nm.

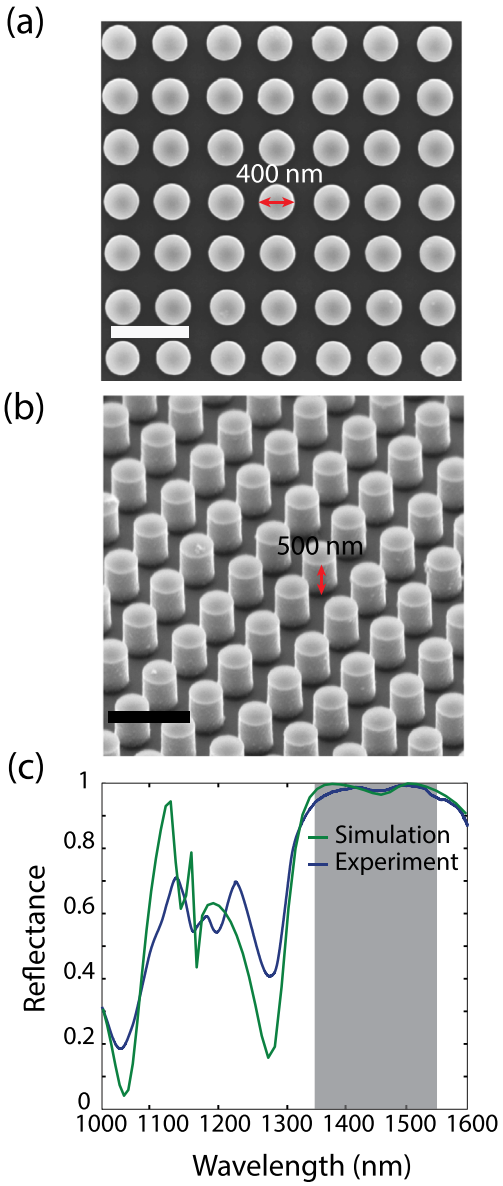

FIG. 3. (a) Top and (b) isometric SEM images of periodic Si cylinder-based MMs. The scale bars in the images are equal to 1 μm. (c) Comparison between the numerically calculated and measured reflectance spectra of the MMs. The average reflectance between 1355 nm and 1555 nm (grey shaded region) is over 98.0%.

(RIE) to create the arrays of Si cylinders with a diameter of $D = 400$ nm and height of $H = 500$ nm (Figs. 3(a) and 3(b)).

The reflectance from the periodic MM was measured with white light at normal incidence and is compared with the simulated reflectance in Fig. 3(c). The simulated reflectance was calculated using dispersive Si optical properties which were measured using ellipsometry. To properly compare with the measured spectra, the simulations include a 2 μm SiO_2 layer below the Si resonators and a semi-infinite Si substrate. The maximum measured reflectance is 99.3% at 1503 nm and the average reflectance is over 98.0% over the wavelength span of 1355 nm to 1555 nm, which is denoted by the grey shaded region in the plot. Moreover, there is excellent agreement between the simulated and measured spectra. It should be noted that the reflectance band is slightly different than in Fig. 2(d) due to the presence of the SiO_2 layer and Si handle wafer below the resonators.

One of the benefits of using MMs over photonic band gap materials is that their response should, ideally, not be a strong function of the periodicity. This is because the resonance is isolated to the unit cell, and the absence of coupling between unit cells ensures that the resonance is not spectrally shifted upon distortion of the lattice. To investigate the effect of periodicity on the perfect reflectors, we have explored the reflectance from disordered arrangements of the cylinders in the MMs. The MMs were designed with periodic 2 by 2 and 3 by 3 resonator supercells and the position of each resonator within the supercell was randomized by offsetting them from their perfectly periodic x and y positions. The exact positions of the resonators for each disorder metamaterial can be found in Table S1 in the supplementary material.[33] The perfectly

periodic positions for each sample are based on a resonator spacing of 660 nm, the same spacing that is used for the MMs presented in Fig. 3. The disorder was quantified by computing the standard deviation in the distances between the four nearest neighbors to each resonator in the supercell and then normalizing this by the periodicity of the perfectly ordered array. MMs with 5 different levels of disorder, equal to 6%, 9%, 15%, 15%, and 17% were modeled and experimentally measured for both E_x and E_y polarizations at normal incidence (Figs. 4(a)–4(e)). Figs. 4(a)–4(d) correspond to 2 by 2 resonator supercells and Fig. 4(e) corresponds to a 3 by 3 resonator supercell configuration. Each MM configuration is illustrated by SEM images of the fabricated structure in the inset of the figure. The reflectance from the disordered structures agrees well with the simulated curves for both polarizations and exhibit a reflection band that is ~180 nm wide. The maximum reflectance value within the band decreases as the percentage disorder increases, with a maximum reflectance of 98.3%, 96.8%, 91.9%, 92.0%, and 86.8% for E_x polarized incidence and 97.1%, 95.8%, 93.1%, 91.0%, and 79.9% for E_y polarized incidence.

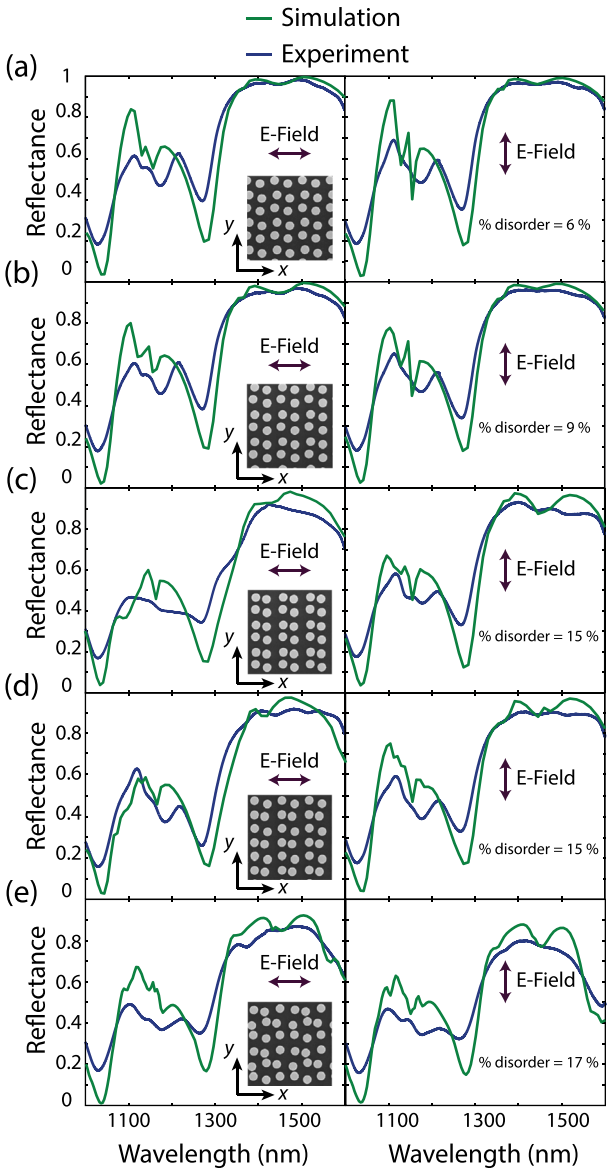

FIG. 4. (a)–(e) Comparison between the simulation and measured reflectance spectra for x and y polarized incidence for MMs with 5 different levels of disorder (6%, 9%, 15%, 15%, and 17%). SEM images of the MMs are shown in the insets. Panels (a)-(d) have 2 by 2 supercells and (e) has a 3 by 3 resonator supercell. The figures indicate a reduction of reflectance with increasing levels of disorder for both polarizations.

The correlation between the strength of disorder and the reduction in reflectance is attributed to spatial variations in the coupling between resonators. For large disorders, cylinders within the supercell have different separations and thus different coupling strengths. Spatial variations in the coupling strengths cause the resonances to shift, leading to spatial variations in ε and μ within the supercell. This is illustrated by the far-field scattering cross-sections of a cylinder dimer, plotted as a function of separation, in Fig. 5(a). It can be observed that narrowing of the gap between the particles leads to blue-shifting of the magnetic dipole resonance, causing it to converge with the electric dipole resonance. Moreover, because the supercell periodicity for the disordered structure is comparable to the wavelength of light within the reflection band, the spatial variations in ε and μ within the supercell lead to the diffraction of light into higher order reflection and transmission modes. This is illustrated in Fig. 5(b) where we plot the calculated total and 0th order (specular) reflection and transmission of the disordered MM corresponding to Fig. 4(e). It can be observed that while the total reflection remains high, the specular reflection is reduced due to loss to higher order modes. This issue is not present in the lightly disordered MMs in Figs. 4(a) and 4(b) as their spacing remains large enough to prevent significant

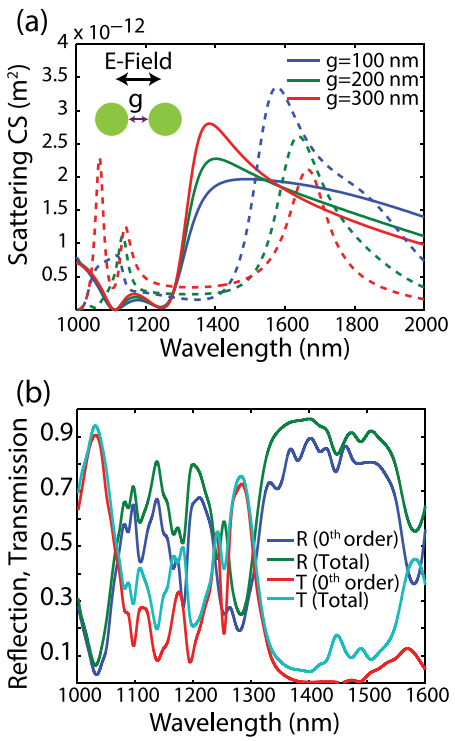

FIG. 5. (a) Scattering cross-sections of Si cylinder dimers as a function of particle spacing. Solid and dashed lines represent the electric and magnetic contributions to the scattering cross-section, respectively. Reduction in the gap size (g) results in a convergence of the resonance positions. (b) Reflection and transmission for a 3 × 3 supercell MM with a disorder of 17%. While the total reflection remains high, light is lost to higher order reflection and transmission modes.

coupling between the resonators. So, while near-perfect reflection from single layer is not limited to periodic structures, the resonators must be prevented from coming in close proximity to one another. It should be noted that this level of control is potentially possible when utilizing nanosphere lithography by managing the electrostatic repulsion between the dielectric spheres used for masking.[30]

One way to reduce the transmission to higher order modes is to utilize a low index substrate. For instance, we found that some of the 0th order reflectance can be recovered by replacing the SiO_2/Si substrate with porous Si with an index of 1.1, which supports fewer diffraction modes. Numerical simulations also showed that the reflection band is maintained across all angles of incidence for *s*-polarized light, and up to a 20° incident angle for *p*-polarized light for ordered MMs. This allows the use of the MM for moderately curved surfaces such as lenses and extreme curvatures or angles of incidence in applications with a well-defined polarization state. More details on this study are given in the supplementary material[33] of this publication.

In summary, we have demonstrated near-perfect reflection from a sub-wavelength-thick Si cylinder-based MM. The observed reflection decreases with lattice disorder due to inhomogeneous material properties and the excitation of higher order modes, though these effects can be partially mitigated by introducing a lower index substrate. The potential to achieve near-perfect reflection with a compact disordered MM may open the door to large-area fabrication using low-cost and high-throughput patterning techniques such as nanosphere lithography and synthesis by self-assembly.

This work was funded by the Office of Naval Research (ONR) under program N00014-12-1-0571 (Vanderbilt University) and N00014-12-1-0722 (SRI International). A portion of this research was conducted at the Center for Nanophase Materials Sciences, which is sponsored at Oak Ridge National Laboratory by the Scientific User Facilities Division, Office of Basic Energy Sciences, U.S. Department of Energy. Scanning electron microscopies were performed in part through the use of the VUMC Cell Imaging Shared Resource. The authors thank Dr. Colby Bellew of SRI for design help.

[1]R. A. Shelby, D. R. Smith, and S. Schultz, Science **292**, 77 (2001).
[2]V. M. Shalaev, W. Cai, U. K. Chettiar, H.-K. Yuan, A. K. Sarychev, V. P. Drachev, and A. V. Kildishev, Opt. Lett. **30**, 3356 (2005).
[3]S. Zhang, W. Fan, N. Panoiu, K. Malloy, R. Osgood, and S. Brueck, Phys. Rev. Lett. **95**, 137404 (2005).
[4]J. Valentine, S. Zhang, T. Zentgraf, E. Ulin-Avila, D. A. Genov, G. Bartal, and X. Zhang, Nature **455**, 376 (2008).
[5]D. Smith, W. Padilla, D. Vier, S. Nemat-Nasser, and S. Schultz, Phys. Rev. Lett. **84**, 4184 (2000).
[6]M. Choi, S. H. Lee, Y. Kim, S. B. Kang, J. Shin, M. H. Kwak, K.-Y. Kang, Y.-H. Lee, N. Park, and B. Min, Nature **470**, 369 (2011).
[7]P. Moitra, Y. Yang, Z. Anderson, I. I. Kravchenko, D. P. Briggs, and J. Valentine, Nat. Photonics **7**, 791 (2013).
[8]X. Huang, Y. Lai, Z. H. Hang, H. Zheng, and C. T. Chan, Nature Mater. **10**, 582 (2011).
[9]C. M. Soukoulis and M. Wegener, Nat. Photonics **5**, 523 (2011).
[10]A. Boltasseva and H. A. Atwater, Science **331**, 290 (2011).
[11]N. I. Zheludev, Science **328**, 582 (2010).
[12]J. Zhou, T. Koschny, M. Kafesaki, E. N. Economou, J. B. Pendry, and C. M. Soukoulis, Phys. Rev. Lett. **95**, 223902 (2005).
[13]K. Vynck, D. Felbacq, E. Centeno, A. Căbuz, D. Cassagne, and B. Guizal, Phys. Rev. Lett. **102**, 133901 (2009).
[14]B.-I. Popa and S. Cummer, Phys. Rev. Lett. **100**, 207401 (2008).
[15]Q. Zhao, J. Zhou, F. Zhang, and D. Lippens, Mater. Today **12**, 60 (2009).
[16]A. B. Evlyukhin, C. Reinhardt, A. Seidel, B. S. Luk'yanchuk, and B. N. Chichkov, Phys. Rev. B **82**, 045404 (2010).
[17]J. C. Ginn, I. Brener, D. W. Peters, J. R. Wendt, J. O. Stevens, P. F. Hines, L. I. Basilio, L. K. Warne, J. F. Ihlefeld, P. G. Clem, and M. B. Sinclair, Phys. Rev. Lett. **108**, 097402 (2012).
[18]C. L. Holloway, E. F. Kuester, J. Baker-Jarvis, and P. Kabos, IEEE Trans. Antennas Propag. **51**, 2596 (2003).
[19]S. O'Brien and J. B. Pendry, J. Phys.: Condens. Matter **14**, 6383 (2002).
[20]C. F. Bohren and D. R. Huffman, *Absorption and Scattering of Light by Small Particles* (John Wiley & Sons, 1983).
[21]Y. H. Fu, A. I. Kuznetsov, A. E. Miroshnichenko, Y. F. Yu, and B. Luk'yanchuk, Nat. Commun. **4**, 1527 (2013).
[22]A. García-Etxarri, R. Gómez-Medina, L. S. Froufe-Pérez, C. López, L. Chantada, F. Scheffold, J. Aizpurua, M. Nieto-Vesperinas, and J. J. Sáenz, Opt. Express **19**, 4815 (2011).
[23]L. Peng, L. Ran, H. Chen, H. Zhang, J. Kong, and T. Grzegorczyk, Phys. Rev. Lett. **98**, 157403 (2007).
[24]I. Staude, A. E. Miroshnichenko, M. Decker, N. T. Fofang, S. Liu, E. Gonzales, J. Dominguez, T. S. Luk, D. N. Neshev, I. Brener, and Y. Kivshar, ACS Nano **7**, 7824 (2013).
[25]B. Slovick, Z. G. Yu, M. Berding, and S. Krishnamurthy, Phys. Rev. B **88**, 165116 (2013).
[26]L. Shi, J. T. Harris, R. Fenollosa, I. Rodriguez, X. Lu, B. A. Korgel, and F. Meseguer, Nat. Commun. **4**, 1904 (2013).
[27]Y. Tang and A. E. Cohen, Phys. Rev. Lett. **104**, 163901 (2010).
[28]E. Yablonovitch, J. Opt. Soc. Am. B **10**, 283 (1993).
[29]P. Hanarp, M. Käll, and D. S. Sutherland, J. Phys. Chem. B **107**, 5768 (2003).
[30]C. L. Haynes, A. D. McFarland, M. T. Smith, J. C. Hulteen, and R. P. Van Duyne, J. Phys. Chem. B **106**, 1898 (2002).
[31]L. I. Basilio, L. K. Warne, W. L. Langston, W. A. Johnson, and M. B. Sinclair, IEEE Antennas Wireless Propag. Lett. **11**, 113 (2012).
[32]L. K. Warne, L. I. Basilio, W. L. Langston, W. A. Johnson, and M. B. Sinclair, Prog. Electromagn. Res. B **44**, 1 (2012).
[33]See supplementary material at http://dx.doi.org/10.1063/1.4873521 for more information.
[34]X. Chen, T. Grzegorczyk, B.-I. Wu, J. Pacheco, and J. Kong, Phys. Rev. E **70**, 016608 (2004).
[35]D. R. Smith, D. C. Vier, T. Koschny, and C. M. Soukoulis, Phys. Rev. E **71**, 036617 (2005).
[36]Z. Szabo, G.-H. Park, R. Hedge, and E.-P. Li, IEEE Trans. Microwave Theory Tech. **58**, 2646 (2010).